THE ASTROPHYSICAL JOURNAL, 399:634–645, 1992 November 10

ON THE EVOLUTION OF SLOWLY ACCRETING NEUTRON STARS

O. M. BLAES
Canadian Institute for Theoretical Astrophysics, University of Toronto, 60 St. George Street, Toronto, ON, Canada M5S 1A1
R. D. BLANDFORD
Theoretical Astrophysics 130-33, California Institute of Technology, Pasadena, CA 91125
P. MADAU
Department of Physics and Astronomy, The Johns Hopkins University; and Space Telescope Science Institute, 3700 San Martin Drive, Baltimore, MD 21218
AND
L. YAN
Theoretical Astrophysics 130-33, California Institute of Technology, Pasadena, CA 91125
Received 1992 March 4; accepted 1992 May 18

ABSTRACT

In the light of recent calculations of pycnonuclear reaction rates for light elements, we reconsider the problem of slow interstellar accretion onto old, possibly magnetized neutron stars. We argue that accretion will occur at the Hoyle-Lyttleton rate after the star has spun down in $\lesssim 10^9$ yr. A deep ocean of liquid hydrogen and helium, extending down to depths ~ 100 m, will cover the surface of the star once it has accreted $\sim 10^{25}$ g of gas. Beneath the ocean will be a layer of almost pure solid ^{16}O which undergoes two-stage electron capture to ^{16}C above a pressure 2.7×10^{28} dyne cm^{-2}, corresponding to an accreted mass of $\sim 10^{27}$ g. The accreted material will then be potentially vulnerable to elastic Rayleigh-Taylor instability with the old underlying crust below. Taking into account the presence of multiple layers of distinct chemical composition, we conclude that the crust will be stable to small perturbations under the conditions envisaged for instellar accretion. A thick layer of up to 10^{27} g of metastable ^{16}C will then accumulate. Seismic waves could possibly be released if finite amplitude perturbations are applied or by some other unspecified quake mechanism. They will generally transfer energy into the magnetosphere in the form of relativistic shear Alfvén waves, in spite of the presence of the deep ocean. We discuss the implications of these results to old Galactic neutron stars as sources of gamma-ray bursts. We find that *any* planar distribution of sources with *any* luminosity function produces a unique relationship between the source counts and the sky distribution, which is inconsistent with the BATSE data. Wide LMXBs and neutron stars in molecular clouds may also accrete under the circumstances described.

Subject headings: accretion, accretion disks — dense matter — gamma rays: bursts — nuclear reactions, nucleosynthesis, abundances — stars: neutron

1. INTRODUCTION

Ever since the discovery of Her X-1 and Cen X-3 by the *Uhuru* satellite, it has been realized that accreting neutron stars can be prodigious sources of X-rays. These sources, which are generally found in close binary systems, are widely supposed to be accreting at rates $\sim 10^{14}$–10^{18} g s^{-1}, high enough to ensure that nuclear statistical equilibrium is maintained in the crust either as a consequence of steady burning or intermittent thermonuclear flashes (e.g., Joss 1977). By contrast, isolated neutron stars, and those with companions which undergo minimal mass loss, accrete at a sufficiently slow rate, $10^8 \lesssim \dot{M} \lesssim 10^{13}$ g s^{-1}, that thermonuclear reactions do not occur and a large reservoir of nuclear energy can accumulate. However, under the high-pressure conditions in the crust of a neutron star, slow pycnonuclear transformations can take place. In addition, the large electron Fermi energies encountered in this environment allow the neutron excesses within the nuclei to increase and, consequently, the mean molecular weights to change discontinuously. Density inversions are then likely to develop which may be reservoirs of stored gravitational potential energy, as well as nuclear energy.

In two earlier papers, Blaes et al. (1989, 1990, hereafter Papers I and II), we investigated some physical processes which, we believe, are relevant to understanding slow accretion onto a cold neutron star. The primary motivation for this study as well as for many parallel analyses (reviewed, for example, in Higdon & Lingenfelter 1990) was to explain gamma-ray bursts (GRBs). These were widely suspected to be associated with local neutron stars. However, the BATSE experiment on the *Compton Gamma-Ray Observatory* has reported an isotropic sky distribution and an apparent deficiency of weak events (Meegan et al. 1992). This is inconsistent with a Galactic disk neutron star origin, and thus with our slow accretion model (see Appendix A). Alternatively, it might be possible for the new data to be interpreted in terms of a Galactic model in which the luminosity function varies spatially. It is quite clear that GRBs do not constitute a homogeneous population; the three soft repeaters and the ~ 12 *Ginga* and *Konus* cyclotron line bursts exhibiting anomalous energy spectra and spatial anisotropy respectively (Schaefer 1991).

Whatever the outcome of this ongoing debate, the question remains as to what are the observational signatures of slow accretion as there must be at least $\sim 10^4$ neutron stars within ~ 300 pc accreting gas at rates of less than 10^{13} g s^{-1}. In Paper I, we argued that impulsive release of energy in the deep crust of a magnetized neutron star would generate seismic waves.

These would propagate to the surface and be temporarily trapped by a reflecting layer, leaking slowly into the magnetosphere as relativistic Alfvén waves. It was also shown that the hydromagnetic wave energy might plausibly be converted into γ-rays and some specific mechanisms by which this might occur were outlined. In Paper II, a specific energy source was proposed: as density inversions develop in the solid crust and exceed a critical magnitude, an elastic Rayleigh-Taylor instability occurs, converting latent gravitational energy into mechanical energy and heat, possibly triggering a thermonuclear flash.

In the present paper, our intention is to update and extend the results of the previous two investigations, incorporating recent computations of pycnonuclear reaction rates. In § 2, we reconsider the problem of interstellar accretion onto old neutron stars. This is followed in § 3 by a reexamination of the nuclear evolution of a slowly settling crust. In § 4, some new results on the elastic Rayleigh-Taylor instability are presented, and in § 5, we reconsider seismic wave propagation in the crust model derived in § 3. Our conclusions are collected in § 6.

2. INTERSTELLAR ACCRETION ONTO NEUTRON STARS

Hydrodynamical accretion from the interstellar medium onto the surface of a neutron star occurs at the rate

$$\dot{M} \simeq 10^{10} v_{40}^{-3} n_{\rm ISM} \text{ g s}^{-1} , \quad (1)$$

where v_{40} is the speed of the star relative to the ISM in units of 40 km s^{-1}, and $n_{\rm ISM}$ is the hydrogen number density of the interstellar gas in cm^{-3} (Hoyle & Lyttleton 1939). (Throughout this paper we assume neutron stars of radius $R = 10$ km, mass 1.4 $M_\odot$, and surface gravity $g = 2 \times 10^{14}$ cm s^{-2}.) With the chosen scalings the total mass accreted over 10 Gyr is $\simeq 10^{-6} M_\odot$. As discussed in Paper II, the weight of the infalling material will compress the outer crust to a pressure $p \simeq 10^{28}$ dyne cm^{-2}, alter its original nuclear composition, and make it depart from nuclear equilibrium. These numbers are confirmed by more detailed Monte Carlo calculations of neutron star accretion. Taking into account the velocity distribution at birth inferred for radio pulsars, as well as the ISM space and density distributions, Blaes & Rajagopal (1991) find that the mean accreted mass after 10 Gyr for neutron stars in the solar vicinity is $\sim 4 \times 10^{-7} M_\odot$.

Equation (1) is only valid when the collision mean free path in the ambient gas is smaller than the accretion radius

$$r_B = 1.2 \times 10^{13} v_{40}^{-2} \text{ cm} . \quad (2)$$

The collision cross section between neutral hydrogen atoms is $\sim 3 \times 10^{-16}$ cm^2 so that, even in a molecular cloud with $n_{\rm ISM} \simeq 100$ cm^{-2}, the fluid limit applies for neutral hydrogen only when $v_{40} < 0.6$. In a more tenuous interstellar environment, only an ionized plasma will accrete at the fluid rate. A neutron star with a surface temperature $\gtrsim 10^5$ K will radiate ionizing photons at a rate $\gtrsim 10^{39}$ s^{-1}, sufficient to ionize the incoming flow beyond the accretion radius for $v_{40} > 0.1$ (Alcock & Illarionov 1980). Note that the accretion itself can self-consistently keep the surface temperature high enough for this to be true. It is in this regime that hydrodynamical accretion onto old, isolated neutron stars can proceed at the rate given in equation (1).

Observations of pulsars suggest that the star magnetic fields decay with a time scale $\lesssim 10^7$ yr (Lyne, Manchester, & Taylor 1985), although there is some evidence for a long-lived "residual" component (Kulkarni 1986). The accretion flow onto a spinning, magnetized neutron star must overcome two obstacles. Suppose the star has a dipolar field $B \simeq 10^{12} B_{12}$ G, a rotation period Ps, and slows down at the magnetic dipole rate. At first, accretion will proceed provided that the ram pressure of the incoming gas at the accretion radius exceeds the pulsar momentum flux. Adopting the magnetic dipole formula for neutron star spin-down, we find that the rotation period must satisfy

$$P \gtrsim P_B \simeq 9.5 B_{12}^{1/2} \dot{M}_{10}^{-1/4} v_{40}^{-1/4} \text{ s} , \quad (3)$$

where $\dot{M}_{10} \equiv \dot{M}/(10^{10}$ g s$^{-1})$. This will occur after a time $t \simeq 6 B_{12}^{-1} \dot{M}_{10}^{-1/2} v_{40}^{-1/2}$ Gyr. The decay of the stellar dipole moment will further facilitate accretion.

Once accretion can proceed inside the accretion radius, the ram pressure will increase $\propto r^{-5/2}$, whereas the pulsar momentum flux will increase $\propto r^{-2}$, so that the inflow will not be resisted. However, a new stress balance can be established within the neutron star light cylinder when the Reynolds stress exerted by the accreting matter balances the Maxwell magnetic stress of the dipolar field at the Alfvén radius, r_A. The details of this interaction are still controversial (Davies, Fabian, & Pringle 1979). However, as long as the star spins faster than the Keplerian angular frequency at the Alfvén radius, a lower bound to the matter stress is given by $\rho(GM/r_A)$ [the maximum stress that can be exerted is approximately $\rho\Omega(GMr_A)^{1/2}$]. Solving for r_A we obtain

$$r_A \simeq 3.4 \times 10^{10} B_{12}^{4/7} \dot{M}_{10}^{-2/7} \text{ cm} . \quad (4)$$

The torque acting on the star, $G_A = \dot{M}(GMr_A)^{1/2}$ will cause its rotational energy to decay on a time scale $t_A \simeq 2\pi I/(P_B G_A) \sim 0.8 B_{12}^{-11/14} \dot{M}_{10}^{-17/28} v_{40}^{1/4}$ Gyr (where $I \simeq 10^{45}$ g cm^2 is the star's moment of inertia), until corotation is achieved at a period

$$P_C \simeq 3 \times 10^3 B_{12}^{6/7} \dot{M}_{10}^{-3/7} \text{ s} . \quad (5)$$

Only at this point will accretion finally be able to proceed. In view of the scalings in equation (5), we believe that isolated, magnetized neutron stars older than ~ 1 Gyr should rotate very slowly and accrete interstellar gas at the rate given by equation (1).

3. NUCLEAR EVOLUTION OF THE OUTER CRUST

In this section, we reconsider the evolution of accreted interstellar gas on the surface of a neutron star. We confine our attention to slow rates of accretion so that the temperature is too low to allow thermonuclear rearrangement of the nuclei. Although the accreted material may initially be confined by the magnetic field, we expect that it will spread horizontally and cover the surface before pycnonuclear and electron capture reactions become important (Paper II). We therefore consider the accretion to be spherically symmetric. Spallation reactions at the surface of the star are likely to destroy most of the metals in the accreting gas leaving just hydrogen and helium (Bildsten, Salpeter, & Wasserman 1991). Initially, this gas is supposed to rest upon a primordial neutron star crust that was originally in nuclear equilibrium as either ^{56}Fe or ^{62}Ni.

The accreted layer will be steadily crushed by the weight of freshly accreted gas and will sink relative to the surface. In Paper II, we described and estimated how the hydrogen will be transformed through pycnonuclear reactions and/or electron capture to form ^{4}He (see also Hameury et al. 1982; Hameury, Heyvaerts, & Bonazzola 1983). Recent, more detailed calculations by Zdunik et al. (1992) confirm these estimates and

indicate that the accreted layer will be mostly converted to ^{4}He at densities ranging from $\sim 10^6$ g cm^{-3} for $\dot{M}_{10} \sim 1$, to the hydrogen electron capture threshold 1.2×10^7 g cm^{-3} for higher accretion rates. For ordinary neutron stars, thermonuclear reactions lead to unstable burning layers when $\dot{M}_{10} \gtrsim 2 \times 10^3$. Stars with pion condensed cores require $\dot{M}_{10} \gtrsim 7 \times 10^4$. We are only interested in stars accreting below these critical rates.

At the above densities, the crust is effectively isothermal with temperature $\simeq 10^6 \dot{M}_{10}^{5/11}$ K. The classical melting point for a charge Z ionic lattice is $\simeq 1.3 \times 10^3 Z^{5/3} (\rho/\mu_e)^{1/3}$ K (Slattery, Doolen, & DeWitt 1982), so the helium layer is expected to solidify at a density of $\sim 3 \times 10^7 \dot{M}_{10}^{15/11}$ g cm^{-3}. Even at zero temperature, however, zero-point fluctuations imply that helium must form a quantum liquid above a certain critical density ρ_c (Yakovlev & Shalybkov 1989), an important effect which was neglected in Paper II. Mochkovitch & Hansen (1979) find $\rho_c(^4\text{He}) \simeq 3 \times 10^8$ g cm^{-3}, while Ceperley & Alder (1980) find only $\simeq 7 \times 10^7$ g cm^{-3}. Between the classical and quantum liquid phases, a layer of solid helium will therefore be present for mass accretion rates $\dot{M}_{10} < 2 - 5$, which is in the expected regime for average interstellar accretion. The hydrogen layer on top will also form a quantum liquid above a density $\rho_c(^1\text{H}) \simeq 2\text{–}6 \times 10^4$ g cm^{-3}. The melting temperature at this density is only 3–5 $\times 10^4$ K, so unless the accretion rate is extremely low, $\dot{M}_{10} \lesssim 10^{-3}$, the hydrogen layer will be completely liquid throughout.

Beyond the conversion to helium, the evolution of the accreted material depends upon the detailed pycnonuclear reaction rates (which were uncertain at the time of writing of Paper II). New computations by Schramm & Koonin (1990) and Schramm, Langanke & Koonin (1991) have affirmed the Salpeter & van Horn (1969) reaction rates for binuclear reactions in a solid lattice and given a triple-α reaction rate for a pure helium liquid which we have fitted to

$$\frac{dn_C}{dt} = K_C n_{He}^3 \exp\left(-\beta_C n^{-1/6}\right), \quad (6)$$

with $K_C = 7.1 \times 10^{-43}$ cm^6 s^{-1} and $\beta_C = 1.71 \times 10^7$ cm$^{-1/2}$. This triple-α rate is numerically similar to that calculated earlier by Fushiki & Lamb (1987) and is valid in the range $3 \times 10^8 \lesssim \rho \lesssim 10^9$ g cm^{-3} of interest to us. Along with $^{12}\text{C}(\alpha, \gamma)^{16}\text{O}$, this reaction is so rapid that helium will be significantly depleted before further (α, γ) reactions can process the accreted material to heavier nuclei.[1] We are therefore left with a nuclear evolution in the accreted layer very similar to Figure 4 of Paper II, leaving ^{16}O as the dominant element at densities greater than 10^9 g cm^{-3}.

Even if the reaction rates still turn out to be somewhat inaccurate, the composition at the bottom of the accreted layer will remain almost pure ^{16}O anyway. This is because gravitational settling is very effective. Any nucleus with a higher mean molecular weight per electron $\mu_e \simeq A/Z$ than ^{4}He will sink in the ocean. Species like ^{12}C or ^{16}O have slightly smaller μ_e than ^{4}He because of their greater binding energies, and would therefore have a tendency to float if the ions were supported purely by Coulomb interactions with the degenerate electrons.[2] The effect is very small, however, and the ion pressure p_{He} must be taken into account. Hameury, Heyvaerts, & Bonazzola (1983) have studied this problem in the case where p_{He} is thermal in origin. Here p_{He} is more likely to be $\sim n_{He} \hbar \omega_{pHe}$, where $\omega_{pHe} \simeq 1.3 \times 10^3 n_{He}^{1/2}$ rad s^{-1} is the helium ion plasma frequency. The relative upward force between oxygen and helium nuclei is approximately

$$F_O - F_{He} \simeq \frac{g m_u}{Z_{He}} \left[\frac{Z_O Z_{He}}{m_u} \left(\frac{\Delta M_{He}}{Z_{He}} - \frac{\Delta M_O}{Z_O} \right) - \left(\frac{\partial p_{He}/\partial n_{He}}{\partial p/\partial n_e} \right) (A_O - A_{He}) \right], \quad (7)$$

where ΔM is the mass excess of the relevant nucleus. Numerically, this equation requires

$$\frac{\partial p_{He}/\partial n_{He}}{\partial p/\partial n_e} \sim 5 \times 10^{-8} n_{He}^{1/6} > 2.6 \times 10^{-3} \quad (8)$$

in order for oxygen to sink. If our estimate for the ion pressure is correct, this is easily satisfied at the ambient densities $\sim 5 \times 10^8$ g cm^{-3} of interest in the ocean. Adopting a diffusion coefficient of $\sim \omega_{pHe} n_{He}^{-2/3}$, the settling time scale at depth $\sim 10^4$ cm is then ~ 40 yr.

Any carbon nucleus which forms in the liquid helium quickly (in ~ 1 ns) captures an α particle to form ^{16}O. The time scale for further α captures to form neon is $\sim 10^8$ yr, many orders of magnitude larger than our uncertain estimate of the settling time scale. Hence no more reactions can occur before the oxygen nuclei settle out to form a solid sediment at the bottom of the ocean. If a solid helium layer is present above the quantum liquid phase, then any metals at the melting interface (apart from ^{12}C), which were present in the original accreted plasma or which were formed by pycnonuclear reactions in the solid, will also diffuse down to the ocean floor unchanged by further reaction.

We have calculated the pycnonuclear evolution of the accreted layer after the formation of ^{4}He adopting the reaction rates of Schramm & Koonin (1990)[3] and Schramm, Langanke, & Koonin (1991), and assuming that at the relevant densities the equation of state is adequately described by extremely relativistic electron degeneracy (eq. [18] of Paper II). Our reaction rate parameters are given in Table 1, which should be compared with Table 2 of Paper II. We integrated the rate equations downward until the top of the quantum ocean was reached and found that pycnonuclear reactions in initially pure solid helium contribute at most 0.1% heavy element concentration by mass (for $\dot{M}_{10} > 10^{-2}$) down to the melting point. We then integrated the total oxygen production rate in the ocean, and dumped all the ^{16}O which was formed down onto the bottom. As accretion proceeded and the accreted layer was further compressed, the ocean thickened until a steady state

[1] An even faster triple-α rate is found in a more recent calculation by Müller & Langanke (1991) due largely to the ^{8}Be resonance at 92 keV, which becomes relevant at a density of $\sim 3 \times 10^9$ g cm^{-3}. However, their rate is in agreement with equation (6) for densities below $\sim 10^9$ g cm^{-3}.

[2] We are grateful to the referee, B. Paczyński, for enlightening us on the subtleties of this issue.

[3] See eq. (33) in their paper. We assumed a bcc lattice and used the parameters in the last row of their Table 1, which correspond to the relaxed approximation to the interaction potential and to the enhanced effective mass of the two fusing ions due to lattice polarization. We also included the wave function curvature factor ~ 0.1.

TABLE 1

PYCNONUCLEAR REACTION PARAMETERS

Reaction	S Factor (MeV barns)	K	β (10^7 cm$^{-1/2}$)
^{4}He(2α, γ)^{12}C	...	7.1×10^{-43} cm^6 s^{-1}	1.71
^{12}C(α, γ)^{16}O	...	9.0×10^{15} cm$^{7/4}$ s^{-1}	1.19
^{16}O(α, γ)^{20}Ne	0.39	1.8×10^{3} cm$^{7/4}$ s^{-1}	1.77
^{20}Ne(α, γ)^{24}Mg	8.6×10^{7}	4.3×10^{11} cm$^{7/4}$ s^{-1}	2.02
^{24}Mg(α, γ)^{28}Si	2.1×10^{10}	1.1×10^{14} cm$^{7/4}$ s^{-1}	2.25
^{28}Si(α, γ)^{32}S	1.1×10^{11}	6.0×10^{14} cm$^{7/4}$ s^{-1}	2.45

was reached where helium entering the top of the ocean was balanced by oxygen production and sedimentation to the bottom. We found that the physical conditions at the bottom of this steady state ocean are nearly independent of accretion rate, as shown in Figure 1.

As described in Paper II, after $\sim 5\dot{M}_{10}^{-1}$ Gyr the ^{16}O layer will reach down to a pressure 2.7×10^{28} dyne cm^{-2}. Adopting an S-factor of 2.3×10^{27} MeV barns (Fowler, Caughlan, & Zimmerman 1975), the ^{16}O + ^{16}O pycnonuclear reaction time scale at this pressure is $\sim 10^{23}$ yr, so ^{16}O will in fact survive down to this point. Two-stage electron capture will then occur to ^{16}C, resulting in a density inversion with the layer below. These electron captures will also reduce the Coulomb barrier. The time scale for ^{16}C to undergo pycnonuclear reactions is uncertain because of the unknown S-factor. Assuming it is comparable to that for ^{12}C + ^{12}C (Koonin 1991, private communication), i.e., 8.8×10^{16} MeV barns (Fowler, Caughlan, & Zimmerman 1975), we estimate that most of the ^{16}C will be processed to heavier elements at pressures ranging from (2–4) $\times 10^{29}$ dyne cm^{-2} for $\dot{M}_{10} \sim 10^{-2}$–$10^{3}$. The time required for this to occur is less than 10^{10} yr for $\dot{M}_{10} \gtrsim 4$. Before these pressures are reached, the accreted layer may buckle due to the density inversion, a scenario to which we turn our attention in the next section. If the layer remains stable, however, this further nuclear evolution may occur. Additional potentially unstable layers might then develop due to electron captures onto the nuclear products.

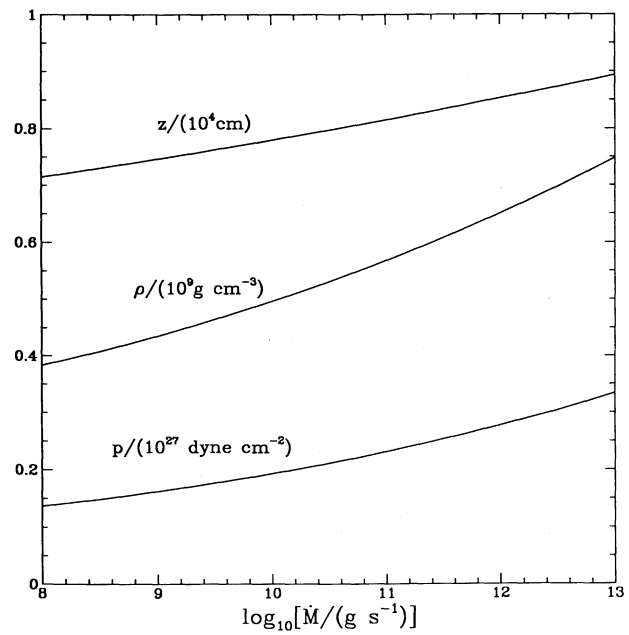

FIG. 1.—Accretion rate dependence of the depth, density, and pressure at the bottom of the helium ocean once it has reached a steady state with the oxygen sediment below. The hydrogen layer above has been neglected, and extreme relativistic electron degeneracy has been assumed, which produce inaccuracies of at most 10 m in the depth.

4. ELASTIC RAYLEIGH-TAYLOR INSTABILITY

In Paper II we investigated the elastic stability of a relativistically degenerate neutron star crust with overdense layers. The model consisted of a plane-parallel layer of finite thickness resting on an infinitely thick layer of different composition. The shear modulus was taken to be that of a bcc lattice and was assumed, for simplicity, not to vary across the interface. An unstable mode was found for a finite range of horizontal wavenumbers provided that the overdensity at the interface exceeded a critical value of

$$\frac{\rho_1 - \rho_2}{\rho_2} \simeq 0.078\left(\frac{\mu/p}{0.024}\right). \quad (9)$$

Here the subscripts 1 and 2 refer to the upper and lower layers, respectively, μ is the shear modulus, and we have scaled μ/p with a value appropriate for an ion charge of $Z = 26$. In general, $\mu/p = 0.024(Z/26)^{2/3}$ (Baym & Pines 1971).

However, when the composition changes, μ/p will differ on either side of the interface, and it is interesting to determine how this effect changes the instability criterion. We have recomputed this criterion for a $(Z = 6)/(Z = 26)$ interface using the correct value of μ/p for both bcc lattices (0.009 and 0.024, respectively). We find that $[(\rho_1 - \rho_2)/\rho_2]_{\rm crit} \simeq 0.065$. A ^{16}C/^{62}Fe interface with $[(\rho_1 - \rho_2)/\rho_2] = 0.118$ would still be unstable. The sense of this change is easy to understand. Reducing the shear modulus of the upper layer renders it more fluid-like and consequently more prone to instability. The effect is not especially large.

A more serious modification is to include multiple interfaces between layers of different composition that will be present in a realistic neutron star crust. From the previous section, we expect a density inversion comprising ^{16}C, which is formed by electron capture, resting on top of the primordial crust which probably consists of ^{56}Ti, ^{62}Cr, or ^{62}Fe. The corresponding relative density jumps are 0.05, 0.03, and 0.12, respectively. Above the ^{16}C layer is ^{16}O and the relative density change is -0.25. This extra layer is expected to produce a stabilizing influence relative to the two-layer problem because it reduces the overdensity in an average sense.

We have considered the instability of a three-layer plane-parallel crust comprising ^{16}O (layer 1), resting on ^{16}C (layer 2), which is again resting on ^{62}Fe (layer 3). Depth is scaled so that the C/Fe interface is at a distance $z = 1$ below the surface; the O/C interface is at $z = z_i$. Pressures and densities are scaled with their values just above the C/Fe interface. The equilibrium pressure and density distributions are then given by

$$p(z) = \begin{cases} \left[\dfrac{r_{12} z}{1 + z_i(r_{12} - 1)}\right]^4, & 0 \le z \le z_i, \\ (z + z_i r_{12} - z_i)^4, & z_i \le z \le 1, \\ \left[1 + \dfrac{z - 1}{r_{23}(1 + z_i r_{12} - z_i)}\right]^4, & z \ge 1, \end{cases} \quad (10)$$

$$\rho(z) = \begin{cases} r_{12}\left(\dfrac{r_{12}z}{1 + z_i r_{12} - z_i}\right)^3, & 0 \le z \le z_i, \\ \left(\dfrac{z + z_i r_{12} - z_i}{1 + z_i r_{12} - z_i}\right)^3, & z_i \le z \le 1, \\ \dfrac{1}{r_{23}}\left[1 + \dfrac{z - 1}{r_{23}(1 + z_i r_{12} - z_i)}\right]^3, & z \ge 1, \end{cases} \quad (11)$$

where $r_{12} \equiv \rho(^{16}\mathrm{O})/\rho(^{16}\mathrm{C})$ and $r_{23} \equiv \rho(^{16}\mathrm{C})/\rho(^{62}\mathrm{Fe})$, at the upper and lower interfaces, respectively.

The linearized perturbation equations, boundary conditions, and numerical method of solution are derived and discussed in Paper II. (The equations of motion are also presented in Appendix B, including the effect of a magnetic field; this is sufficiently small that we may neglect it here.) We used the same equations and method for this three-layer equilibrium. In particular, all perturbations were assumed to have a time and horizontal spatial dependence of the form $\exp[i(k_x x - \omega t)]$.

In our numerical explorations we found that only one mode, if any, is unstable in three-layer equilibria, like those that might arise in a neutron star crust. In Figure 2 we present the dispersion relations $\omega^2(k_x)$ of this mode for the $^{16}\mathrm{O}/^{16}\mathrm{C}/^{62}\mathrm{Fe}$ equilibrium with different values of the $^{16}\mathrm{O}$ layer thickness z_i. The shear moduli in the three layers are given by $\mu/p = 0.011$ ($^{16}\mathrm{O}$), 0.009 ($^{16}\mathrm{C}$), and 0.024 ($^{62}\mathrm{Fe}$), while the density ratios are $r_{12} = 0.75$ and $r_{23} = 1.118$. This equilibrium is stable for $z_i > 0.78$. Note that with a single layer of $^{16}\mathrm{C}$ resting on $^{62}\mathrm{Fe}$, we found in Paper II that the interface was highly unstable, as the density change $\rho(^{16}\mathrm{C})/\rho(^{62}\mathrm{Fe}) = 1.118$ is much greater than the critical value $r_{\mathrm{crit}} = 1.078$. However, a layer of $^{16}\mathrm{O}$ resting on top of the $^{16}\mathrm{C}$ has a stabilizing influence as the density change at the $^{16}\mathrm{O}/^{16}\mathrm{C}$ interface is 0.75. We find that if the thickness of the $^{16}\mathrm{O}$ layer is more than 0.78 (that is $z_i \ge 0.78$), then there are no longer any unstable modes. Hence a substantial thickness of $^{16}\mathrm{C}$ must be built up in order for instability to occur.

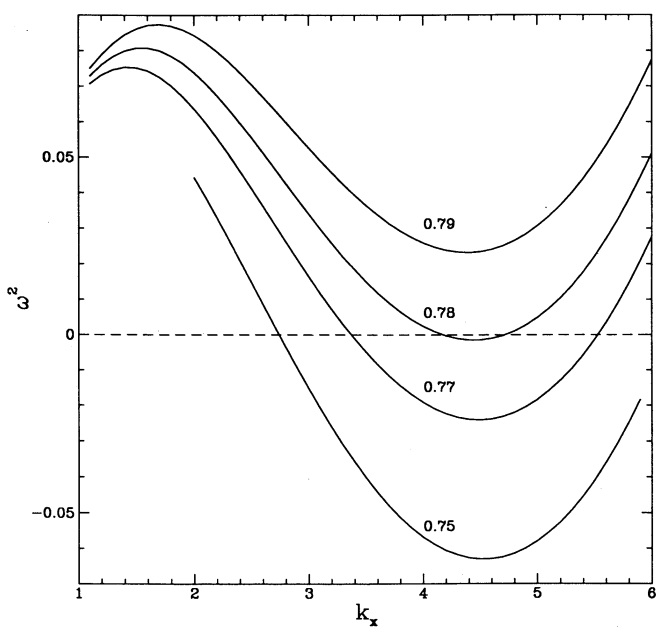

FIG. 2.—Dispersion relations $\omega^2(k_x)$ for the $^{16}\mathrm{O}/^{16}\mathrm{C}/^{62}\mathrm{Fe}$ equilibrium. Each curve is labeled with the chosen thickness of the $^{16}\mathrm{O}$ layer, measured relative to the depth of the interface between $^{16}\mathrm{C}$ and $^{62}\mathrm{Fe}$.

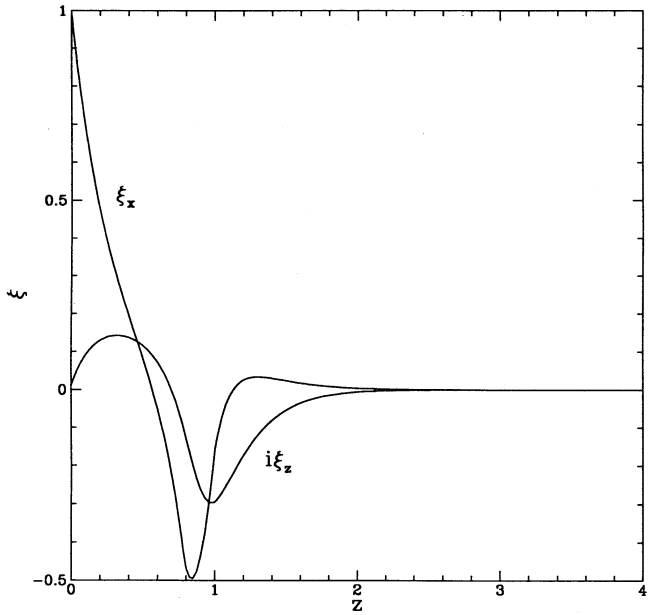

FIG. 3.—Displacement components for the unstable mode for $k_x = 4.5$ and $z_{31} = 0.77$. The vertical scale is chosen so that $\xi_x = 1$ at the surface.

Figure 3 shows the eigenfunctions for $k_x = 4.5$ in the unstable equilibrium with $z_i = 0.77$. The vertical displacement ξ_z is concentrated around the $^{16}\mathrm{C}/^{62}\mathrm{Fe}$ interface at $z = 1$, as is the derivative in the horizontal displacement ξ_x. This behavior is similar to the two-layer case with large unstable density ratios, illustrated in Figure 7*b* of Paper II. The presence of the extra interface at $z = z_i$ appears to have had an effect, however, in increasing the number of nodes in the eigenfunctions over those of the two-layer case. We have searched unsuccessfully for modes with fewer numbers of nodes which might be expected to be more unstable. Moreover, we followed the behavior of this mode as z_i is decreased and found that the number of nodes decreased as z_i approaches zero. There is therefore a continuity in the eigenfunctions between the two- and three-layer equilibria as z_i varies.

Equilibria with z_i less than the critical thickness of 0.78 are in fact unphysical, as the pressure at the $^{16}\mathrm{C}/^{62}\mathrm{Fe}$ interface then exceeds the electron capture threshold for $^{62}\mathrm{Fe}$ to form $^{62}\mathrm{Cr}$. (In fact the $^{62}\mathrm{Fe}$ layer, even when it can exist, must have a finite thickness down to its electron capture threshold, and this will presumably have a further stabilizing effect.) We have also studied equilibria in which $^{62}\mathrm{Cr}$ and $^{56}\mathrm{Ti}$ formed the underlying primordial crust and found no unstable modes. This is not surprising given that the relative overdensities at the lower interface are only 3% and 5% respectively, and the two-layer calculations therefore predict a stable equilibrium.

We conclude that even those neutron stars which accrete enough material to get beyond the electron capture threshold of $^{16}\mathrm{O}$ will have multiply layered crusts which are mechanically stable to small perturbations.

5. ENERGY TRANSMISSION TO THE MAGNETOSPHERE

If mechanical energy is suddenly released deep inside the neutron star crust (where the magnetic field is negligible), elastic waves will be radiated and will propagate throughout the star. As discussed in Paper I, this wave energy will be stored for many dynamical times as it slowly leaks out into the magnetosphere in the form of Alfvén waves. The energy trans-

mission coefficient for shear waves in the solid crust was calculated, as these couple more efficiently to the magnetosphere than do compressional waves. However, we have shown above that many neutron stars will have fluid surfaces, due either to quantum melting of the helium layer or indeed to thermal melting of the hydrogen and helium layers. At first sight it would appear that the bottom of these oceans are so deep that the surface magnetic fields would not supply any significant shear stress in the fluid layers. Therefore one expects only compressional waves to be able to propagate to the surface. Surprisingly, this is not, in fact, true as we shall now describe.

In contrast to the previous section, we expect small variations in the mean molecular weight per electron, μ_e, to be of little consequence in determining wave transmission properties, so we shall take $\mu_e = 2$ throughout the crust. The density structure is then given by equation (2) of Paper I. The ion charge Z is potentially more important as it determines the shear modulus μ. However, $\mu = 0$ in the ocean where elements lighter than oxygen are to be found, and it seems reasonable to take $Z = 26$ as a typical value in the deeper, solid layers.

As in Paper I we shall start by considering vertically propagating waves. Including a magnetic field, the equations of motion for elastic waves in plane-parallel geometry are

$$\frac{d}{dz}\left[\left(\mu + \frac{B^2\cos^2\alpha}{4\pi}\right)\frac{d\xi_x}{dz}\right] - \frac{B^2\sin\alpha\cos\alpha}{4\pi}\frac{d^2\xi_z}{dz^2} + \omega^2\left[\left(\rho + \frac{B^2\cos^2\alpha}{4\pi c^2}\right)\xi_x - \frac{B^2\sin\alpha\cos\alpha}{4\pi c^2}\xi_z\right] = 0\ ; \quad (12)$$

$$\frac{d}{dz}\left[\left(\mu + \frac{B^2\cos^2\alpha}{4\pi}\right)\frac{d\xi_y}{dz}\right] + \omega^2\left(\rho + \frac{B^2}{4\pi c^2}\right)\xi_y = 0\ ; \quad (13)$$

$$\frac{d}{dz}\left[\left(\frac{4\mu}{3} + \frac{B^2\sin^2\alpha}{4\pi} + \rho\frac{dp}{d\rho}\right)\frac{d\xi_z}{dz}\right] - \frac{B^2\sin\alpha\cos\alpha}{4\pi}\frac{d^2\xi_x}{dz^2} + \omega^2\left[\left(\rho + \frac{B^2\sin^2\alpha}{4\pi c^2}\right)\xi_z - \frac{B^2\sin\alpha\cos\alpha}{4\pi c^2}\xi_x\right] = 0\ , \quad (14)$$

where, as in the previous section, we have assumed a time dependence of the wave variables of the form $\exp(-i\omega t)$. Note that we have changed notation from the previous section to be consistent with Paper I: z is now the height above the surface. We have taken the magnetic field to be uniform and in the x-z plane at angle α to the vertical. Deep in the crust, the magnetic field becomes unimportant and equations (12)–(14) have asymptotic solutions

$$\xi_x \sim |z|^{-7/4}\{A_{Isx}\exp[-i(u_s + \omega t)] + A_{Rsx}\exp[i(u_s - \omega t)]\}\ , \quad (15)$$

$$\xi_y \sim |z|^{-7/4}\{A_{Isy}\exp[-i(u_s + \omega t)] + A_{Rsy}\exp[i(u_s - \omega t)]\}\ , \quad (16)$$

$$\xi_z \sim |z|^{-7/4}\{A_{Ic}\exp[-i(u_c + \omega t)] + A_{Rc}\exp[i(u_c - \omega t)]\}\ , \quad (17)$$

where

$$u_s \equiv -\int^z dz\,\frac{\omega}{v_s}\ , \quad (18)$$

$$u_c \equiv -\int^z dz\,\frac{\omega}{v_c}\ , \quad (19)$$

and $v_s = (\mu/\rho)^{1/2}$ and $v_c = (dp/d\rho + 4\mu/3\rho)^{1/2}$ are the shear and compressional wave speeds, respectively. Equations (15)–(17) describe the usual elastic wave modes: two shear and one compressional. The A_I's and A_R's represent complex incident and reflected wave amplitudes, respectively.

The ξ_y shear waves propagate independently of the other wave modes and turn into Alfvén waves when the magnetic field becomes dominant,

$$\xi_y = A_{Ta}\exp\left[i\omega\left(\sec\alpha\,\frac{z}{c} - t\right)\right]\ , \quad (20)$$

where A_{Ta} is the complex amplitude of the transmitted relativistic Alfvén wave. This is the wave transmission problem which was analyzed in Paper I in the case of a purely solid crust.

If $\alpha \neq 0$, then as the magnetic field becomes dominant it couples the ξ_z compressional wave with the ξ_x shear wave to produce fast and slow magnetosonic modes. In fact, in the magnetosphere, equations (12) and (14) both imply

$$\xi_\perp \equiv \xi_z\sin\alpha - \xi_x\cos\alpha = A_{Tf}\exp\left[i\omega\left(\frac{z}{c} - t\right)\right]\ , \quad (21)$$

where A_{Tf} is the complex amplitude of the transmitted relativistic fast wave, with displacement $\xi_\perp$ orthogonal to the magnetic field. Because there is no restoring force along the magnetic field in the magnetosphere, we have lost the slow mode and the parallel component of the displacement, $\xi_\parallel \equiv \xi_z\cos\alpha + \xi_x\sin\alpha$, is completely free.

Before solving equations (12)–(14), we still need boundary conditions at the bottom of the ocean, where μ goes discontinuously to zero. These are continuity in vertical displacement ξ_z, continuity in horizontal displacements ξ_x and ξ_y (because of the required continuity in tangential electric field), and finally continuity in the vertical components of the stress on the perturbed surface

$$\left[\left(\mu + \frac{B^2\cos^2\alpha}{4\pi}\right)\frac{d\xi_x}{dz} - \frac{B^2\sin\alpha\cos\alpha}{4\pi}\frac{d\xi_z}{dz}\right] = 0\ , \quad (22)$$

$$\left[\left(\mu + \frac{B^2\cos^2\alpha}{4\pi}\right)\frac{d\xi_y}{dz}\right] = 0\ , \quad (23)$$

$$\left[\left(\frac{4\mu}{3} + \frac{B^2\sin^2\alpha}{4\pi} + \rho\frac{dp}{d\rho}\right)\frac{d\xi_z}{dz} - \frac{B^2\sin\alpha\cos\alpha}{4\pi}\frac{d\xi_x}{dz}\right] = 0\ . \quad (24)$$

Using the same method described in Paper I, we have integrated equations (12)–(14) numerically using equations (15)–(24) as boundary conditions in order to determine the transmitted and reflected wave amplitudes for each of the three incident wave modes. The transmission coefficient was then computed using the energy flux formulae described in Appendix B. Our results are presented in Figures 4 and 5.

It is clear that the ocean produces a large modulation of the transmission coefficient for both shear wave polarizations. This is because it acts as an interference filter for shear waves, allowing certain frequencies to be transmitted very effectively. The

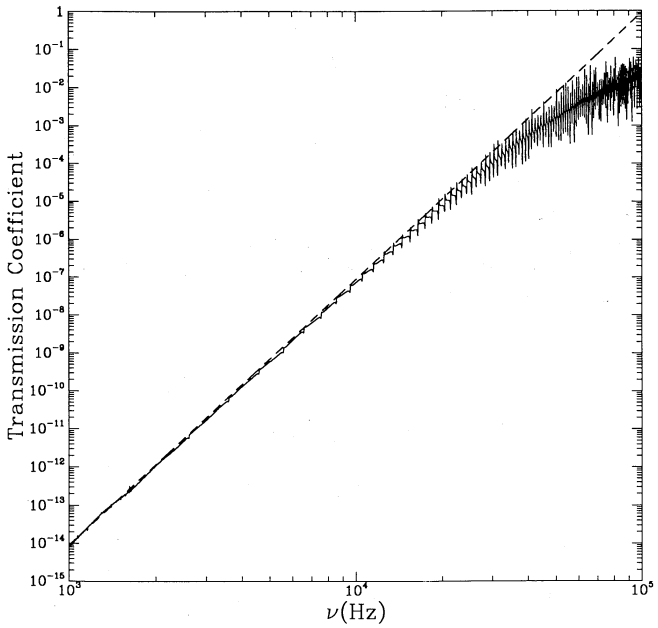

FIG. 4.—Transmission coefficient for vertically propagating compressional waves through an ocean of depth 80 m. The magnetic field strength is taken to be 10^{12} G and is at an angle of 45° to the vertical. The dashed line is the low-frequency approximation given by eq. (25).

difference between successive "resonant" frequencies is the reciprocal of twice the Alfvén wave crossing time in the ocean, $\Delta\nu \simeq 5v_A(z_{oc})\cos\alpha/(4z_{oc})$, where $v_A = (B^2/4\pi\rho)^{1/2}$ and z_{oc} is the depth of the ocean bottom.

Because the shear modulus is typically only a few percent of the pressure, compressional waves are relatively unaffected by the ocean (although wiggles and spikes are evident in Figure 4 at the same resonant frequencies). The compressional wave transmission coefficient may therefore be estimated in a similar manner to the estimate for the shear wave transmission coefficient presented in Paper I. At low frequencies we find

$$T_c \simeq 1.8 \times 10^{-14} \sin^2\alpha \left(\frac{B}{10^{12}\ \mathrm{G}}\right)^2 \left(\frac{\nu}{10^3\ \mathrm{Hz}}\right)^7 \times \left(\frac{\mu_e}{2}\right)^{-4} \left(\frac{g}{2\times 10^{14}\ \mathrm{cm\ s^{-2}}}\right)^{-7} . \quad (25)$$

This is also plotted in Figure 4 and clearly provides a good fit at low frequencies. Combining T_c with the two-way crossing time through the crust, the compressional wave storage time in the crust is

$$\tau_c \sim \frac{900}{\sin^2\alpha}\left(\frac{\nu}{10^4\ \mathrm{Hz}}\right)^{-7}\left(\frac{B}{10^{12}\ \mathrm{G}}\right)^{-2}\left(\frac{z_Q}{10^3\ \mathrm{m}}\right)^{1/2} \times \left(\frac{\mu_e}{2}\right)^4 \left(\frac{g}{2\times 10^{14}\ \mathrm{cm\ s^{-2}}}\right)^{13/2} \mathrm{s}\ , \quad (26)$$

where z_Q is the depth of the seismic wave source. Contrast this with the low-frequency storage time for shear waves in a purely solid crust (see Paper I, eq. [33]),

$$\tau_s \sim \frac{7000}{\cos\alpha}\left(\frac{\nu}{10^3\ \mathrm{Hz}}\right)^{-7}\left(\frac{B}{10^{12}\ \mathrm{G}}\right)^{-2}\left(\frac{z_Q}{10^3\ \mathrm{m}}\right)^{1/2} \times \left(\frac{\mu_e}{2}\right)^4 \left(\frac{g}{2\times 10^{14}\ \mathrm{cm\ s^{-2}}}\right)^{13/2} \left(\frac{Z}{26}\right)^{7/3} \mathrm{s}\ , \quad (27)$$

Thus compressional waves transmit energy much more slowly than do shear waves in the absence of an ocean.

At low frequencies, the presence of the ocean actually increases the transmission coefficient of shear waves, as indicated in Figure 5*b*. This may be understood by considering the

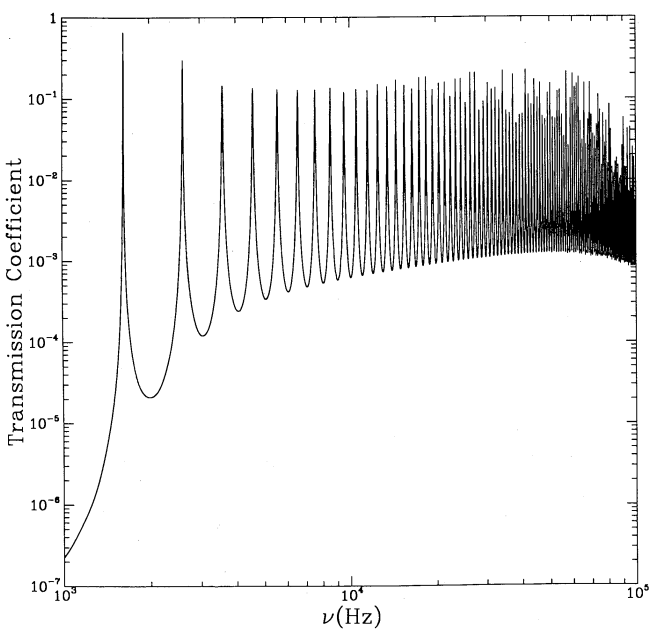

FIG. 5*a*

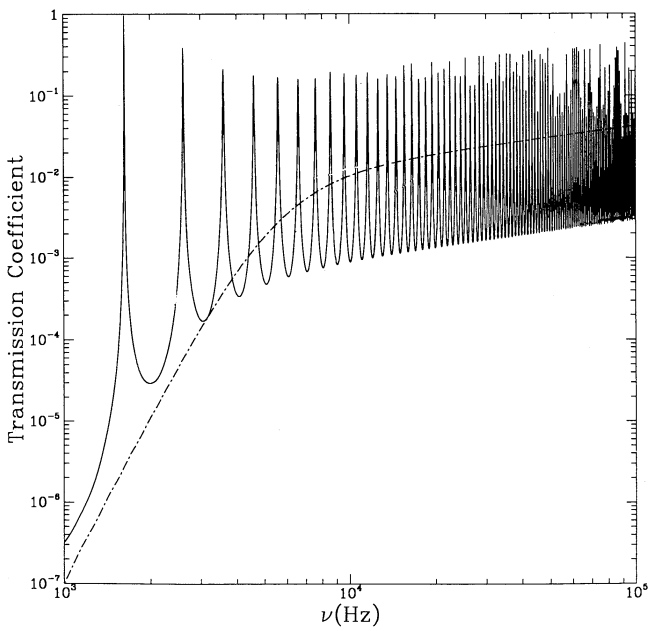

FIG. 5*b*

FIG. 5.—As in Fig. 4 but for incident shear waves polarized with displacement (*a*) in the plane of the magnetic field and the vertical and (*b*) orthogonal to this plane. The dot-dashed curve in the latter figure is the transmission coefficient in the absence of any ocean.

shear wave impedances in the solid crust, $Z_C \sim (\rho\mu)^{1/2}$; the ocean, $Z_O \sim [\rho B^2 \cos^2 \alpha/(4\pi)]^{1/2}$; and the magnetosphere, $Z_M = B^2 \cos \alpha/(4\pi c)$. Generally $Z_C \gg Z_O \gg Z_M$. Transmission is a two-stage process from the solid phase to the ocean and then from the ocean to the magnetosphere. Waves propagating to the surface have to pass through an evanescent zone (Paper I) at depth z_{ev}. This is below the ocean bottom z_{oc} for

$$\nu < 2.8 \times 10^3 \left(\frac{z_{oc}}{80 \text{ m}}\right)^{-1/2} \times \left(\frac{g}{2 \times 10^{14} \text{ cm s}^{-2}}\right)^{1/2} \left(\frac{Z}{26}\right)^{1/3} \text{Hz} . \quad (28)$$

In this regime, the transmission coefficient is approximately $4[Z_O(z_{oc})/Z_C(z_{ev})][Z_M/Z_O(z_c)]$, where z_c is a characteristic depth in the ocean where the propagation speed changes on a length scale of order a wavelength (see Paper I). Because Z_O increases with depth, the ocean improves the overall impedance match and the wave transmission coefficient is larger. At higher frequencies, there is no evanescent zone in the solid phase and the transmission coefficient is $\sim 4[Z_O(z_{oc})/Z_C(z_{oc})][Z_M/Z_O(z_c)]$. Waves in the solid are therefore forced to couple at the ocean bottom, which is deeper than where they would be able to couple had there been no ocean. The impedance mismatch is therefore made worse by the ocean, and transmission decreases.

The two-way crossing time from the quake depth to the ocean bottom is $\simeq 0.8(z_Q^{1/2} - z_{oc}^{1/2})/[(10^3 \text{ m})^{1/2} - (80 \text{ m})^{1/2}]$ ms, while the two-way crossing time from the ocean bottom to the surface is $\simeq 0.7(z_{oc}/80 \text{ m})(B \cos \alpha/10^{12} \text{ G})^{-1}$ ms. Dividing the total by the transmission coefficient gives the shear wave storage time, which from Figure 5 is ~ 6000 s at 10^3 Hz and ~ 0.6 s at 10^5 Hz.

The main conclusion to draw from Figures 4 and 5 is that, given the estimated helium ocean depths, low-frequency ($\lesssim 3 \times 10^4$ Hz for $B = 10^{12}$ G) shear waves can still be transmitted faster than vertically propagating compressional waves. Moreover, because of the isotropic dispersion relation of relativistic fast waves, compressional waves with significant angles of incidence to the surface will produce negligible transmission into the magnetosphere (Paper I, McDermott et al. 1984). This will also be true for the shear wave modes with displacements in the plane of the vertical and magnetic field, because they also couple only to fast modes. The orthogonal shear wave modes couple instead to anisotropic relativistic Alfvén waves, and we expect that their transmission coefficient will have a relatively weak dependence on the angle of incidence.

The conclusions of Paper I remain essentially unchanged. After a glitch or a starquake, the wave energy in the crust will slowly leak into the magnetosphere, producing relativistic Alfvén waves. The presence of an ocean will merely slow down the overall transmission rate. Note that if a solid layer exists within the ocean as well (because the temperature is so low that ^{4}He can exist in the solid state), then we expect high-frequency shear waves to scatter off this layer, further reducing the transmission coefficient.

Finally, we stress again that the transmission coefficient measures the fractional energy transfer to the magnetosphere every time a wave is incident onto the surface. The remaining energy will be carried off by reflected waves which will eventually return to the surface provided they are not damped on the crossing time scale (Paper I). The transmission coefficient is *not* a measure of the efficiency of energy transfer (see Harding 1991 and Hartmann 1991) as *all* the wave energy can eventually leak out into the magnetosphere in the absence of competitive dissipation. A low transmission coefficient merely increases the storage time of wave energy in the crust.

6. DISCUSSION

In this paper, we have revised and developed an analysis of slow interstellar accretion onto neutron stars. We now turn to a brief summary of the observational ramifications. There are three immediate possibilities to consider, γ-ray bursts, neutron stars in wide binaries, and isolated neutron stars in molecular clouds.

6.1. *γ-Ray Bursters*

The original motivation for the research presented in Papers I and II and the current paper was to examine neutron starquake models of GRBs. However, the discovery that GRBs appear to be isotropic on the sky, while maintaining sub-Euclidean source counts appears to be incompatible with a local neutron star origin as originally envisaged (see Appendix A). It has been argued, though, that the subset of GRBs that exhibit cyclotron lines may be anisotropic on the sky and consequently associated with the Galaxy (Schaefer 1991). If so, they may be accreting neutron stars. It is of interest that none of the GRBs, except the soft repeater GB 790305, show convincing evidence for rotation. This is consistent with the model of interstellar accretion developed in § 2, in which it was concluded that the star had to be spun down to unobservably slow rotation ($P \sim 1$ hr) in order for it to accrete appreciable quantities of interstellar gas. Detection of rapid rotation in just one GRB which exhibits cyclotron lines would surely rule out accretion as a power source as well as a cosmological explanation.

There are further difficulties with the original model. The elastic Rayleigh-Taylor instability proposed in Paper II is shown in §§ 3 and 4 above to be unlikely to operate when the new nuclear reaction rates are adopted and allowing for the variation of shear modulus with atomic number and the finite thickness of the overdense layer. It appears that if there is steady slow accretion onto a neutron star, then a thick layer of up to $\sim 10^{27}$g of metastable (with respect to mechanical and nuclear equilibrium) ^{16}C will accumulate. (This carbon may be subject to further binuclear reaction.) However, the thickness of this layer is probably insufficient to satisfy the formal linear instability criterion. It remains possible, as discussed in Paper II, that a thin, overdense layer could become unstable as a result of the application of stress to the equilibrium configuration, thereby releasing the latent gravitational energy impulsively. However, if the temperature is raised to a sufficient value to initiate nuclear burning, then it is likely that a burning front will propagate all around the star and release up to 10^{44} ergs. Such bursts could be seen as far away as ~ 5 Mpc, but would be anisotropically distributed.

As noted by Paczyński (1991), a halo distribution of bursting neutron stars with sufficiently large core radius (> 17 kpc) may be compatible with the observed isotropy and source counts. The energy released in a typical GRB detected from BATSE, assuming isotropic emission, would then be

$$E_b \simeq 10^{40} \text{ ergs} \left(\frac{F}{10^{-7} \text{ ergs cm}^{-2}}\right)\left(\frac{D}{30 \text{ kpc}}\right)^2 , \quad (29)$$

where F is the observed fluence, and D is the distance.

If halo neutron stars can release free energy (from some unknown source) in the form of a deep crust quake, then the considerations of Paper I still apply here. In this case $E_b \sim \mu d^3 \epsilon_{\rm yield}^2$, where μ is the crustal rigidity, d is a characteristic length associated with the quake, and $\epsilon_{\rm yield}$ is the yield strain. Assuming that the quake occurs over a time scale $\sim d/v_s$, then seismic waves will be released with a typical frequency

$$\nu_0 \simeq 4 \times 10^3 \text{ Hz} \left(\frac{z_Q}{10^3 \text{ m}}\right)^{11/6} \left(\frac{E_b}{10^{40} \text{ ergs}}\right)^{-1/3} \left(\frac{\epsilon_{\rm yield}}{10^{-2}}\right)^{2/3} . \quad (30)$$

From equation (27), the characteristic storage time for wave energy in the crust at this frequency is $\sim 0.5(B/10^{12} \text{ G})^{-2}$ s, comparable with the observed burst durations.

If the number of neutron stars in the halo is comparable with the disk population, we deduce a mean repetition time scale between bursts of

$$\tau \simeq 10^5 \text{ yr} \left(\frac{N}{10^8}\right) \left(\frac{\dot{N}}{800 \text{ yr}^{-1}}\right)^{-1} , \quad (31)$$

where N is the total number of active halo stars, and $\dot{N}$ is the number of bursts observed per year by BATSE. The total amount of energy in γ-rays released by each star over a lifetime of 10^{10} yr is therefore

$$E_{\rm tot} \simeq 10^{45} \text{ ergs} \left(\frac{F}{10^{-7} \text{ ergs cm}^{-2}}\right) \left(\frac{D}{30 \text{ kpc}}\right)^2 \times \left(\frac{N}{10^8}\right)^{-1} \left(\frac{\dot{N}}{800 \text{ yr}^{-1}}\right) . \quad (32)$$

Internal differential rotation between the crustal lattice and the crustal neutron superfluid has been proposed (Epstein 1988) as a possible source of free energy whose sudden release is triggered by the unpinning of vortex lines. In such glitch-powered GRBs, the energy made available by bringing the star into uniform rotation is $E_b \simeq (1/2) I_c \Delta\Omega_{\rm max}^2$, where $I_c \simeq 10^{43}$ g cm^2 is the moment of inertia of the crustal superfluid and $\Delta\Omega_{\rm max}$ is the initial difference in angular velocity which can be supported. To generate 10^{40} ergs in an individual GRB, we require $\Delta\Omega_{\rm max} \gtrsim 0.05$ rad s^{-1}, a value which can easily be supported by the pinning force (Alpar et al. 1984). Note that $\sim \Omega_0/\Delta\Omega_{\rm max} \sim 10^5$ events could then be produced only if $\Omega_0 \gtrsim 6000$ rad s^{-1}, i.e., if the initial period of the rotating neutron star is $\lesssim 1$ ms. However, a smaller value of Ω_0 would be sufficient in the likely case that the neutron star is not brought into uniform rotation each time: in this scenario, after a glitch, the crustal neutron superfluid would rotate with velocity $\Omega + \Delta\Omega_{\rm min}$. The energy available per event would then be $E_b \simeq (\frac{1}{2}) I_c (\Delta\Omega_{\rm max}^2 - \Delta\Omega_{\rm min}^2)$, and $\sim \Omega_0/(\Delta\Omega_{\rm max} - \Delta\Omega_{\rm min})$ GRBs could be generated. It is easy to show that, e.g., $\Omega_0 \simeq 1000$ rad s^{-1} requires $\Delta\Omega_{\rm max} \simeq 0.17$ rad s^{-1}, and $\Delta\Omega_{\rm min} \simeq 0.16$ rad s^{-1}.

6.2. *Neutron Stars in Wide Binaries*

An alternative scenario for slow accretion involves neutron stars in wide binaries, where the mass transfer rate is that associated with main-sequence evolution of the companion. For example, a solar-type star loses mass at a rate $\sim 10^{11}$ g s^{-1} and if a significant fraction of this settles upon an old, neutron star companion, then conditions similar to interstellar accretion might occur. Unfortunately, it is not very likely that there will be a large population of long-period LMXBs as such systems will usually become unbound during the supernova explosion responsible for creating the neutron star, a problem long recognised for the relatively few LMXBs that are observed (see, e.g., Verbunt 1988).

6.3. *Neutron Stars in Molecular Clouds*

Another possibility for producing bursts from slowly accreting neutron stars involves some form of local heating, perhaps following a temporarily high episode of accretion. Passage through a molecular cloud could be responsible, although, again, this would be reflected in the burst distribution on the sky. Presumably, a thermonuclear burning front would propagate around the star consuming all the available nuclear fuel. Hence there would have to be a substantial period of latency between bursts during which the crust can cool and a fresh supply of nuclear fuel accumulate. The energy would likely originate mostly in the liquid helium layer, so the considerations of §§ 4 and 5 would be of little relevance.

The recently discovered pulsating X-ray source H1253+193 is positionally identified with the center of the high Galactic latitude molecular cloud Lynds 1457 (Halpern & Patterson 1987). Although it may be a background cataclysmic variable, as there is an infrared identification (Koyama et al. 1991), it might also represent an example of rapid accretion from a dense molecular cloud. At a distance of 65 pc, the intrinsic X-ray luminosity in the 2–10 keV band, corrected for absorption, is $\sim 10^{31}$ ergs s^{-1}. The soft X-ray luminosity would presumably be somewhat larger, but cannot be measured directly in view of the large hydrogen column density $N_{\rm H} \sim 10^{23}$ cm^{-2} along the line of sight. Adopting, for illustration purposes, a gas density $\sim 10^4$ cm^{-3}, and a neutron star velocity ~ 100 km s^{-1}, we derive from equation (1) a mass accretion rate $\dot{M} \sim 10^{13}$ g s^{-1} and a bolometric luminosity of $\sim 10^{33}$ ergs s^{-1}. The corotation period from equation (5), $P_C \sim 150 B_{12}^{6/7}$ s, is consistent with the observed period of 206 s for a $\lesssim 10^{12}$ G surface magnetic field. At 100 km s^{-1}, the crossing time of the core of the molecular cloud will be ~ 2000 yr and $\sim 5 \times 10^{23}$ g of gas could be accreted, enough material to produce in principle many bursts. If H1253+193 really is a slowly accreting neutron star, then it will be of interest to check if any observed bursts can be positionally associated with it.

The general observability of quiescent and transient emission from slowly accreting neutron stars in the solar neighborhood is the subject of a future paper (Blaes & Madau 1993)

We thank L. Bildsten, A. Hassam, W. Kluźniak, S. Koonin, T. Prince, S. Schramm, F. Thieleman, and S. Woosley for helpful discussions and advice. We are also grateful to the referee, B. Paczyński, for comments which improved a previous version of this paper. R. D. B. is supported by grants AST 89-17765 and NAGW 2372. O. M. B. is supported by the Canadian NSERC.

APPENDIX A

GRB SOURCE COUNTS

A major difficulty with the local neutron star model of GRBs, highlighted by recent observations with the *Gamma-Ray Observatory*, is that the bursts appear to be isotropic on the sky at the same time as exhibiting a non-Euclidean peak counts distribution. In this section, we present a simple model that relates the angular distribution to the source counts that can be used to quantify the discrepancy between the model and the data. In earlier treatments of this problem, (e.g., Hartmann, Epstein, & Woosley 1990; Paczyński 1991) a specific simple model of burst emission is assumed. In particular, it is supposed that the probability that an individual neutron star undergo a burst be independent of location in the Galaxy. This is clearly called into question, particularly if interstellar accretion is ultimately responsible. In addition, the discovery of apparently fast radio pulsars (Frail & Kulkarni 1991; Harrison, Lyne, & Anderson 1992) casts some doubt on the prescriptions used to compute the distribution of old neutron stars in the Galaxy. A third, independent difficulty is that if the majority of GRBs are produced by neutron stars associated with the earliest generations of massive stars, then the scale height of their sources might be considerably greater than that of contemporary radio pulsars.

For all of these reasons, we consider here a very general, local distribution of sources. We place these sources at distances r, supposed small compared with the distance to the Galactic center so that radial gradients in density can be ignored. Let these sources have a luminosity function $\Phi(L, z)$ (per unit volume and per unit L) that depends solely upon luminosity per steradian L and height z above the Galactic plane. The solar system is presumed to be located at $z = 0$. For present purposes, the observed flux $S = L/r^2$ can be replaced with either the directly measured quantity, the peak count rate or the inferred quantity, the fluence. Now define the integral distribution function $N(S, \mu)$ which is the number of sources observed with flux in excess of S and direction cosine to the Galactic pole in excess of μ. We assume that the distribution is symmetric with respect to the Galactic plane and only consider one hemisphere, $0 < \mu < 1$. We can then define the differential distribution function

$$\frac{d^2N}{dS\,d\mu}(S, \mu) = \int_0^\infty dr r^2 \int_0^\infty dL \Phi(L, \mu r)\delta\left(S - \frac{L}{r^2}\right). \tag{A1}$$

This distribution is not yet available. However, information concerning two integrals of it has been released, specifically, the flux distribution averaged over the sky, $dN/dS(S)$ and the angular distribution for sources with flux in excess of some flux limit S_M, $dN/d\mu(\mu)$. These two distributions (treated as positive quantities) are both calculable theoretically from equation (A1).

$$\frac{dN}{dS}(S) = \frac{1}{2S^2}\int_0^{S^{-1/2}} dx G(x)\,, \qquad \frac{dN}{d\mu}(\mu) = \frac{1}{\mu^3}\int_0^{\mu/S_M{}^{1/2}} dx G(x) x^2\,, \tag{A2}$$

where

$$G(x) = \int_0^\infty dL L^{3/2}\Phi(L, xL^{1/2})\,. \tag{A3}$$

The two expressions in equation (A2) can be related. Let us define the integral counts

$$\begin{aligned} N(S) &= -\int_S^\infty dS' \frac{dN(S')}{dS'} \\ &= \frac{1}{2}\int_0^{S^{-1/2}} dx G(x)\left(\frac{1}{S} - x^2\right). \end{aligned} \tag{A4}$$

Hence

$$\left\{\frac{d}{dS}[SN(S)]\right\}_{S_M\mu^{-2}} = \frac{\mu^3}{2}\frac{dN(\mu)}{d\mu}\,. \tag{A5}$$

The source counts averaged over the sky can therefore be used to predict the angular distribution directly and vice versa, independently of the (unknown) luminosity function.

We can draw some conclusions from equation (A5). First, as $dN(\mu)/d\mu < 0$, we conclude that $SN(S)$ must also decrease monotonically. In other words, the slope of the integral source counts must always be less than -1. The BATSE source counts reported by Meegan et al. (1992) have a slope ~ -0.8 and are therefore formally inconsistent with any planar distribution. Second, we can compute the second moment of the angular distribution from a knowledge of the source counts. (The first moment vanishes.) If we denote the Galactic latitude by b, then

$$\begin{aligned} \langle \sin^2 b\rangle &= -\frac{1}{N(S_M)}\int_0^1 d\mu \mu^2 \frac{dN(\mu)}{d\mu} \\ &= 1 - \int_{S_M}^\infty \frac{dS}{S}\frac{N(S)}{N(S_M)} \end{aligned} \tag{A6}$$

after integration by parts. We can also derive an expression for the mean value of $V/V_M \equiv (S/S_M)^{-3/2}$,

$$\left\langle \frac{V}{V_M} \right\rangle = \left(\frac{2}{5}\right) \frac{\int_0^1 d\mu G(\mu S_M^{-1/2})(1-\mu^5)}{\int_0^1 d\mu G(\mu S_M^{-1/2})(1-\mu^2)}, \tag{A7}$$

which always exceeds 0.4. Again, the observed value of 0.348 ± 0.024 (Meegan et al. 1992) is inconsistent with any planar distribution.

We can give an illustration of the use of these formulae by proposing a very simple luminosity function

$$\Phi(L, z) = \Phi_0 e^{-(L+z^2)}, \tag{A8}$$

where both L and z are normalized to fiducial values. We quickly compute

$$G(x) = \frac{3\pi^{1/2}\Phi_0}{4(1+x^2)^{5/2}}. \tag{A9}$$

Hence using equations (A2), we obtain

$$N(S) = \frac{\pi^{1/2}\Phi_0}{4S(1+S)^{1/2}} \qquad S > S_M \qquad N(\mu) = \frac{\pi^{1/2}\Phi_0}{4S_M}\left[(1+S_M)^{-1/2} - \mu(\mu^2+S_M)^{-1/2}\right]. \tag{A10}$$

The counts are roughly compatible with the inferred BATSE counts (although slightly steeper) for $S_M \gtrsim 0.03$. Applying equation (A6), we obtain

$$\langle \sin^2 b \rangle = -S_M + S_M(1+S_M)^{1/2} \sinh^{-1}(S_M^{-1/2}), \tag{A11}$$

which increases monotonically from 0 to $\frac{1}{3}$ as the depth of the survey increases, i.e., as S_M changes from $\gg 1$ to $\ll 1$. For $S_M \sim 0.03$, $\langle \sin^2 b \rangle \sim 0.04$, quite inconsistent with the quoted value of 0.310 ± 0.006 (Meegan et al. 1992). Significantly steeper counts for small S would be necessary to remove this discrepancy with a local disk distribution.

APPENDIX B

LAGRANGIAN FOR MAGNETOELASTIC WAVES

In §§ 4 and 5 we considered perturbations around a static, homentropic equilibrium in an external Newtonian gravitational field. In § 5 we took this equilibrium to have a uniform magnetic field $\boldsymbol{B}$. The equations describing Eulerian perturbations about these equilibria, neglecting dissipation and assuming flux freezing are (see Papers I and II)

$$\rho \frac{\partial^2 \boldsymbol{\xi}}{\partial t^2} = \nabla \cdot \delta\boldsymbol{\sigma} + \frac{\delta\rho}{\rho}\nabla p - \nabla \delta p + \frac{1}{c}\delta\boldsymbol{j} \times \boldsymbol{B}, \tag{B1}$$

$$\delta\sigma_{ij} = \mu\left(\frac{\partial \xi_i}{\partial x_j} + \frac{\partial \xi_j}{\partial x_i} - \frac{2}{3}\delta_{ij}\nabla \cdot \boldsymbol{\xi}\right), \tag{B2}$$

$$\delta\rho = -\nabla \cdot (\rho\boldsymbol{\xi}), \tag{B3}$$

$$\delta p = c_s^2 \delta\rho, \tag{B4}$$

$$\delta\boldsymbol{E} = -\frac{1}{c}\frac{\partial \boldsymbol{\xi}}{\partial t} \times \boldsymbol{B}, \tag{B5}$$

$$\nabla \times \delta\boldsymbol{E} = -\frac{1}{c}\frac{\partial \delta\boldsymbol{B}}{\partial t}, \tag{B6}$$

$$\nabla \times \delta\boldsymbol{B} = \frac{4\pi}{c}\delta\boldsymbol{j} + \frac{1}{c}\frac{\partial \delta\boldsymbol{E}}{\partial t}, \tag{B7}$$

where $c_s^2 \equiv (dp/d\rho)^{1/2}$.

These equations may be combined into a single vector equation for $\boldsymbol{\xi}$, the displacement of a material element from its equilibrium position. We find that this equation may also be derived from the following Lagrangian density,

$$\mathscr{L} = \frac{1}{2}\left(\rho + \frac{B^2}{4\pi c^2}\right)\left(\frac{\partial \boldsymbol{\xi}}{\partial t}\right)^2 - \frac{1}{8\pi c^2}\left(\boldsymbol{B} \cdot \frac{\partial \boldsymbol{\xi}}{\partial t}\right)^2 - \frac{1}{2}(p+\mu)(\nabla_j \xi_i)(\nabla_i \xi_j) - \frac{1}{2}\mu(\nabla_j \xi_i)(\nabla_j \xi_i) - \frac{1}{2}\left(\rho c_s^2 - p - \frac{2}{3}\mu\right)(\nabla \cdot \boldsymbol{\xi})^2$$
$$- \frac{1}{8\pi}(\boldsymbol{B} \cdot \nabla\boldsymbol{\xi})^2 + \frac{1}{4\pi}(\nabla \cdot \boldsymbol{\xi})(\boldsymbol{B} \cdot \nabla)(\boldsymbol{\xi} \cdot \boldsymbol{B}) - \frac{B^2}{16\pi}\left[(\nabla_j \xi_i)(\nabla_i \xi_j) + (\nabla \cdot \boldsymbol{\xi})^2\right]. \tag{B8}$$

In the nonrelativistic limit with zero shear modulus, this becomes the well-known Lagrangian of Dewar (1970). It also agrees with

the variational principle of Paper II (eq. [30]) in the limit of zero magnetic field. From equation (B8), we find that the energy flux

$$q_i = \frac{\partial \xi_j}{\partial t}\left\{ -(p+\mu)(\nabla_j \xi_i) - \mu(\nabla_i \xi_j) - \left(\rho c_s^2 - p - \frac{2}{3}\mu\right)\delta_{ij}\nabla\cdot\boldsymbol{\xi} - \frac{1}{4\pi}B_i B_k \nabla_k \xi_j + \frac{1}{4\pi}B_i B_j \nabla\cdot\boldsymbol{\xi} + \frac{\delta_{ij}}{4\pi}(\boldsymbol{B}\cdot\nabla)(\boldsymbol{\xi}\cdot\boldsymbol{B}) - \frac{B^2}{8\pi}(\nabla_j \xi_i + \delta_{ij}\nabla\cdot\boldsymbol{\xi})\right\}, \quad \text{(B9)}$$

where δ_{ij} is the Kronecker delta. For vertically propagating waves, $\nabla_j = \delta_{jz}\partial/\partial z$ and equation (B9) then gives the wave energy fluxes necessary to calculate the transmission coefficients in § 5.

REFERENCES

Alcock, C., & Illarionov, A. 1980, ApJ, 235, 541
Alpar, M. A., Anderson, P. W., Pines, D., & Shaham, J. 1984, ApJ, 278, 791
Baym, G., & Pines, D. 1971, Ann. Phys., 66, 816
Bildsten, L., Salpeter, E. E., & Wasserman, I. 1992, ApJ, 384, 143
Blaes, O., Blandford, R., Goldreich, P., & Madau, P. 1989, ApJ, 343, 839 (Paper I)
Blaes, O., & Madau, P. 1992, ApJ, in press
Blaes, O., Blandford, R., Madau, P., & Koonin, S. 1990, ApJ, 363, 612 (Paper II)
Blaes, O., & Rajagopal, M. 1991, ApJ, 381, 210
Ceperley, D. M., & Alder, B. J. 1980, Phys. Rev. Lett., 45, 566
Davies, R. E., Fabian, A. C., & Pringle, J. E. 1979, MNRAS, 186, 779
Dewar, R. L. 1970, Phys. Fluids, 13, 2710
Epstein, R. 1988, Phys. Rep., 163, 155
Fowler, W. A., Caughlan, G. R., & Zimmermann, B. A. 1975, ARA&A, 13, 69
Frail, D. A., & Kulkarni, S. R. 1991, Nature, 352, 785
Fushiki, I., & Lamb, D. Q. 1987, ApJ, 317, 368
Halpern, J. P., & Patterson, J. 1987, ApJ, 312, L31
Hameury, J. M., Bonazzola, S., Heyvaerts, J., & Ventura, J. 1982, A&A, 111, 242
Hameury, J. M., Heyvaerts, J., & Bonazzola, S. 1983, A&A, 121, 259
Harding, A. 1991, Phys. Rep., 206, 327
Harrison, P. A., Lyne, A. G., & Anderson, B. 1992, in Proc. ITP Conf. on X-Ray Bursts and the Formation of Binary and Millisecond Pulsars, NATO ASI, ed. E. P. J. van den Heuvel, in press
Hartmann, D. 1991, Ann. N. Y. Acad. Sci., 647, 575
Hartmann, D., Epstein, R. I., & Woosley, S. E. 1990, ApJ, 348, 625
Higdon, J. C., & Lingenfelter, R. E. 1990, ARA&A, 28, 401
Hoyle, F., & Lyttleton, R. A. 1939, Proc. Cambridge Phil. Soc., 35, 592
Joss, P. C. 1977, Nature, 270, 310
Koyama, K., et al. 1991, ApJ, 377, 240
Kulkarni, S. R. 1986, ApJ, 306, L85
Lyne, A. G., Manchester, R. N., & Taylor, J. H. 1985, MNRAS, 213, 613
McDermott, P. N., Savedoff, M. P., Van Horn, H. M., Zweibel, E. G., & Hansen, C. J. 1984, ApJ, 281, 746
Meegan, C. A., Fishman, G. J., Wilson, R. B., Paciesas, W. S., Pendleton, G. N., Horack, J. M., Brock, M. N., & Kouveliotou, C. 1992, Nature, 355, 143
Mochkovitch, R., & Hansen, J. P. 1979, Phys. Lett., 73A, 35
Müller, H.-M., & Langanke, K. 1991, preprint
Paczyński, B. 1991, Acta Astron., 41, 157
Salpeter, E. E., & Van Horn, H. M. 1969, ApJ, 155, 183
Schaefer, B. 1991, Paper Presented at Huntsville Gamma-Ray Burst Workshop (Huntsville, AL, 1991 Oct. 16–18)
Schramm, S., & Koonin, S. E. 1990, ApJ, 365, 296; erratum, 377, 343 (1991)
Schramm, S., Langanke, K., & Koonin, S. E. 1991, preprint
Slattery, W., Doolen, G., & DeWitt, H. 1982, Phys. Rev. A, 26, 2255
Verbunt, F. 1988, Physics of Neutron Stars and Black Holes, ed. Y. Tanaka (Tokyo: Universal Academic), 159
Yakovlev, D. G., & Shalybkov, D. G. 1989, Astrophy. Space Phys. Rev., 7, 311
Zdunik, J. L., Haensel, P., Paczyński, B., & Miralda-Escudé, J. 1992, ApJ, 384, 129